

Heiko Tzschätzsch

Abstract

Medical ultrasound is one of the most common medical imaging modalities. It allows real-time visualization of the morphology of soft tissues in the human body based on backscattered compression waves in the high-frequency (MHz) range. Special technologies are sensitive to organ functions such as blood flow and tissue strain. Over the past decade, ultrasound-based elastography (USE) has been developed and became widely applied in the clinic for the assessment of tissue stiffness in a variety of conditions including malignant tumors and liver fibrosis. The clinical benefit of USE has been overwhelmingly demonstrated in a large number of clinical studies and reviews. Unlike other sonographic methods, USE is not a single technique but rather a set of methodological ideas and approaches centered on the mechanical stimulation of soft tissues, deformation readout, and stiffness reconstruction. This chapter provides an overview of the key concepts of current USE methods and their potential clinical applications. Many of the methods discussed are still experimental, while others have already been replaced by more sophisticated quantitative and image-resolved methods. The aim of this chapter is to guide readers through the pros and cons of individual concepts, thereby helping them to gain insight into the basic principles of USE.

12.1 Introduction

Since the basic developments of medical ultrasound in the 1940s, sonography has become one of the most widely applied diagnostic imaging technique worldwide. The option of real-time data acquisition and intermediate image display, the high

H. Tzschätzsch

Department of Radiology, Charité – Universitätsmedizin Berlin, Berlin, Germany

e-mail: Heiko.Tzschätzsch@charite.de

cost efficiency, the mobility of ultrasound devices, and the possibility of quantifying functional parameters such as flow and marked improvements of detail resolution and image quality over the past years have made sonography the diagnostic imaging modality with the widest dissemination. Since the early 1990s, elastography has been developed as a method to enhance the sensitivity of sonography to mechanical changes caused by pathologies such as benign nodules, malignant tumors, or fibrosis in the human body. The basic image contrast in sonography relates to the compression properties of the tissue, which are determined by the high water content of soft biological tissues and do not vary largely in the body. Elasticity, or more specifically shear elasticity, is measured by controlled imposition and readout of mechanical tissue deformations, followed by somewhat elaborate image processing to reconstruct stiffness maps or *elastograms*. Since the advent of ultrasound elastography (USE), many methods have been devised to address the three key points involved in USE—namely, mechanical stimulation, acquisition of deformation field data, and stiffness image reconstruction. This chapter is a brief introduction to medical ultrasound, the key concepts of USE, and the systems most commonly used to measure shear elasticity by ultrasound.

12.2 Medical Ultrasound

The basic principle of medical ultrasound includes the following steps: 1) generation of sound waves with a transducer, 2) propagation and interaction of these waves with the tissue, 3) acquisition of the reflected waves by the transducer, and 4) reconstruction of an anatomical image from the reflected waves. More insight is gained by considering the three fundamental ultrasound modes — A-mode, M-mode, and B-mode — which will be explained in the following. Additionally, a short introduction to functional ultrasound will be presented.

12.2.1 A-Mode

The *A-mode* (amplitude mode) is the basic and most simple ultrasound mode. Sound, or compression waves, is generated by the piezoelectric element in the head of the transducer (see Fig. 12.1). This element converts electric voltage into mechanical strain (indirect piezoelectric effect). The created compression wave pulse, which is commonly in the megahertz range, propagates from the transducer placed on the skin surface into deeper tissue (in positive x direction) at the speed of sound, $c_{||} = 1540$ m/s (see Table 12.1). There are three main interactions between the propagating compression wave pulse and biological tissues in the body: reflection, scattering, and absorption. Reflection acts at the interface of two tissues with different impedance. The reflection coefficient, R , depends on the relative change of impedance. Due to energy conservation, the corresponding transmission coefficient, T , is given by $T = 1 + R$ (see Chap. 2, Eq. (2.35)). In contrast, scattering acts inside one tissue. The compression

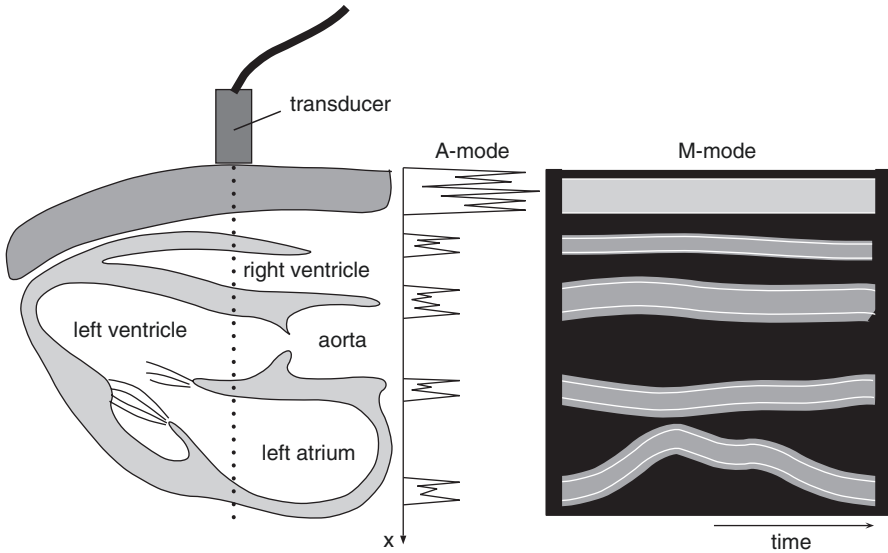


Fig. 12.1 (Left) Setup of single-element transducer and human heart; (middle) corresponding A-mode; (right) M-mode over one cardiac cycle [1]

Table 12.1 Comparison of compression wave speed c_{\parallel} (Eq. (2.22) in Chap. 2) and shear wave c_{\perp} speed (Eq. (2.23) in Chap. 2) of different media, organs, and tissues

Organ	c_{\parallel} in m/s	c_{\perp} in m/s
Air	331	–
Water	1492	–
Breast	1450–1570	1.1–3.5
Liver	1522–1623	0.9–3.0
Brain	1460–1580	1.0–4.6
Thrombus	1586–1597	0.3–1.3
Muscle	1500–1600	1.6–7.6
Bone	1630–4170	1420–3541

Values taken from Sarvazyan et al. [2]

wave scatters at microscopic tissue inhomogeneities. Both effects result in partial reflection and partial transmission of the wave. Absorption causes attenuation of the wave while it propagates through a viscous medium. Wave attenuation has to be compensated for by time-dependent amplification of the received high-frequency signals. Since it is merely an artifact rather than a contrast-generating interaction, absorption of compression waves will not be discussed further. The reflected wave pulse reaches the transducer and will be converted into an electric signal via the direct piezoelectric

effect. The corresponding depth, x , of the reflection can be calculated as the time of flight, Δt , between sending and acquiring the echoes:

$$x = \frac{\Delta t c_{\parallel}}{2}. \quad (12.1)$$

To ensure that no interaction occurs between two wave packages consecutively emitted from the transducer, all echoes of the first pulse must return to the transducer before the next pulse is sent. Therefore, the *pulse repetition frequency* (PRF) is limited by the maximum penetration depth, x_{\max} , through $\text{PRF} = c_{\parallel}/(2 x_{\max})$. Typical values for PRF are in the range of a few thousands of hertz. The magnitude of the reflected wave pulses is related to the anatomical structure and is visualized over the spatial profile (see A-mode in Fig. 12.1).

12.2.2 M-Mode

The *M-mode* (motion mode) is an extension of the A-mode in time. The magnitude of the A-mode is displayed in gray scale over a certain time with the temporal resolution of $1/\text{PRF}$ (see M-mode in Fig. 12.1). High amplitudes of the reflected waves are displayed as hyperintense structures, while tissue regions with few scattering events appear as hypointense areas. Due to its high time resolution, the M-mode is mainly used in echocardiography.

12.2.3 B-Mode

The *B-mode* (brightness mode) is an extension of the A-mode in space. A two-dimensional image is created by the combination of certain A-mode lines with different sector orientation (see Fig. 12.2). For this the transducer consists of an array of piezoelectric elements. For each sector orientation, a so-called *line of sight* (LoS), a certain number of elements are activated simultaneously and act as one element (see Sect. 12.2.1). To acquire the next lateral LoS, another group of elements are activated. In common clinical ultrasound devices, the number n of LoS is in the order of 2^7 – 2^9 . Therefore, the *frame rate* (FR) is reduced to $\text{FR} = \text{PRF}/n$ and is typically in the order of several tens of hertz.

12.2.4 Functional Ultrasound

Unlike anatomical ultrasound, functional ultrasound measures the velocity of fluids like blood and moving tissues such as the cardiac wall. As such functional ultrasound relies on motion encoding based on the Doppler effect or by correlation techniques as explained in Chap. 2, Eq. (2.59).

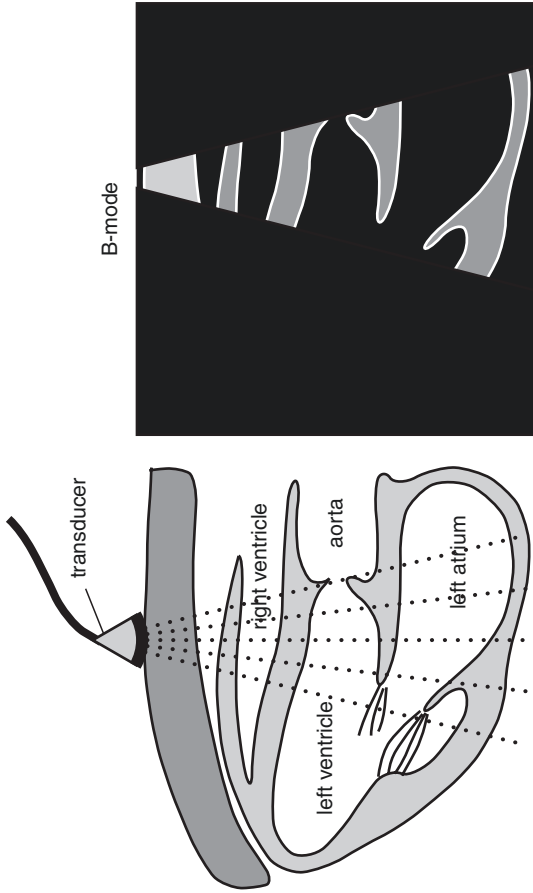


Fig. 12.2 (Left) Setup of multi-element transducer and human heart; (right) corresponding B-mode [1]

12.3 Principles of Ultrasound Elastography

The clinical motivation for developing elastography is lent from palpation. During palpation the physician uses his or her hands to apply a force to the surface of the body and senses the tissue response in terms of hard and soft. However, palpation is subjective and limited to the surface. To overcome these limitations, an elastography experiment uses three major techniques: 1) mechanical stimulation of deep tissue, 2) measurement of deep tissue deformation, and 3) quantification of visco-elastic parameters within the field of view. To understand the basic principles of USE, we briefly introduce, in the next section, four key concepts used by different elastography methods.

12.3.1 Qualitative Elastography

The physical background of palpation is the relationship between the amount of tissue deformation/strain and the applied force/stress. This relationship is in linear elasticity theory defined by Hooke's law (see Chap. 2, Eqs. (2.8) and (2.9)) by which the tissue's shear modulus is defined. Strain can be defined as relative tissue deformation or the gradient of tissue displacement (see Chap. 2, Eq. (2.6)). Strain measured by elastography can be generated by external force or intrinsic motion. The resulting tissue motion can be quantified by cross-correlation techniques similar to the approaches used in the color mode (see Sect. 12.2.4). Strain images are obtained by calculating the spatial derivative from the tissue motion image. The resulting strain map (*elastogram*) shows high strain for soft tissue portions and low strain for stiff tissue portions. Due to the unknown force/stress and boundary conditions, the strain map provides only qualitative information.

12.3.2 ARFI

Strain can be directly generated within the region of interest using a technique known as *acoustic radiation force impulse* (ARFI), which reduces artifacts due to ribs or ascites. ARFI generates a highly focused ultrasound pulse by a controlled delay of the electronic pulse for each single piezoelectric transducer element (see Fig. 12.3) [3]. The ultrasound pulse yields an axially orientated force, which deforms the tissue along the focus direction, thereby generating a laterally propagating shear wave. The resulting shear strain can be measured as described in Sect. 12.3.1. For quantitative elastography, the shear wave propagation speed has to be measured.

12.3.3 Quantitative Elastography

In contrast to strain, the shear wave velocity is independent of the amount of the applied stress and can thus be exploited as a quantitative parameter of the tissue's inherent stiffness (see Table 12.1). Shear waves can be generated in different ways

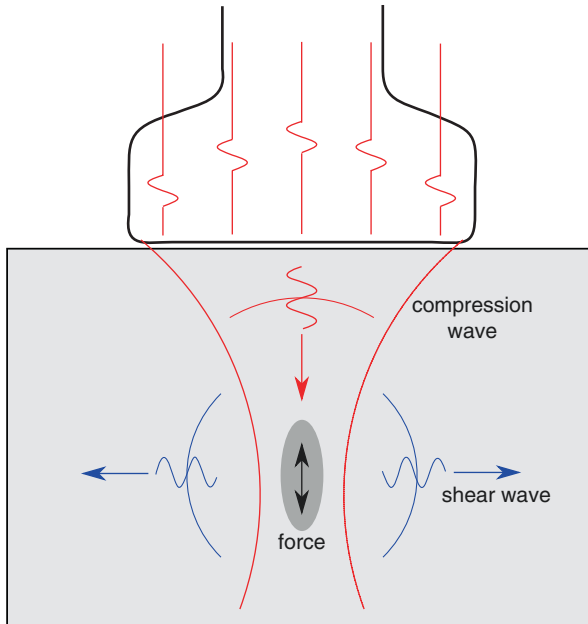


Fig. 12.3 The principle of ARFI. An electric delay between the transducer elements generates a highly focused compression wave, resulting in an axially orientated force within the focus region. The focused force is a new point source which generates a shear wave propagating in lateral direction

(see Fig. 12.4) such as by ARFI (see Fig. 12.3) or using external actuators. Most quantitative ultrasound elastography techniques track the shear wave at different time points and lateral positions. The velocity, which is typically in the order of several m/s, can be estimated using a time-of-flight algorithm. Depending on the specific method used, the shear wave speed is given either as mean value averaged over a small area or as a color-coded elastogram.

12.3.4 Coherent Plane-Wave Compounding

Common ultrasound frame rates are in the order of several tens of hertz. To observe rapid events such as fast shear waves, a higher frame rate is required. The technique of *plane-wave imaging* allows acquisition of B-mode images in a single shot (frame), yielding a frame rate equal to the PRF [4]. This is accomplished by the simultaneous activation of all piezoelectric elements, which generates an unfocused, plane compression wave. To achieve lateral resolution, the backscattered plane waves are acquired with a depth-dependent time delay between signal acquisitions in each piezoelectric element. This approach is called dynamic receive focusing and is similar to the focusing principle shown in Fig. 12.3 but in the receive mode. Due to the loss of focusing in the transmit mode, the improvement in frame rate is achieved at the cost of spatial resolution.

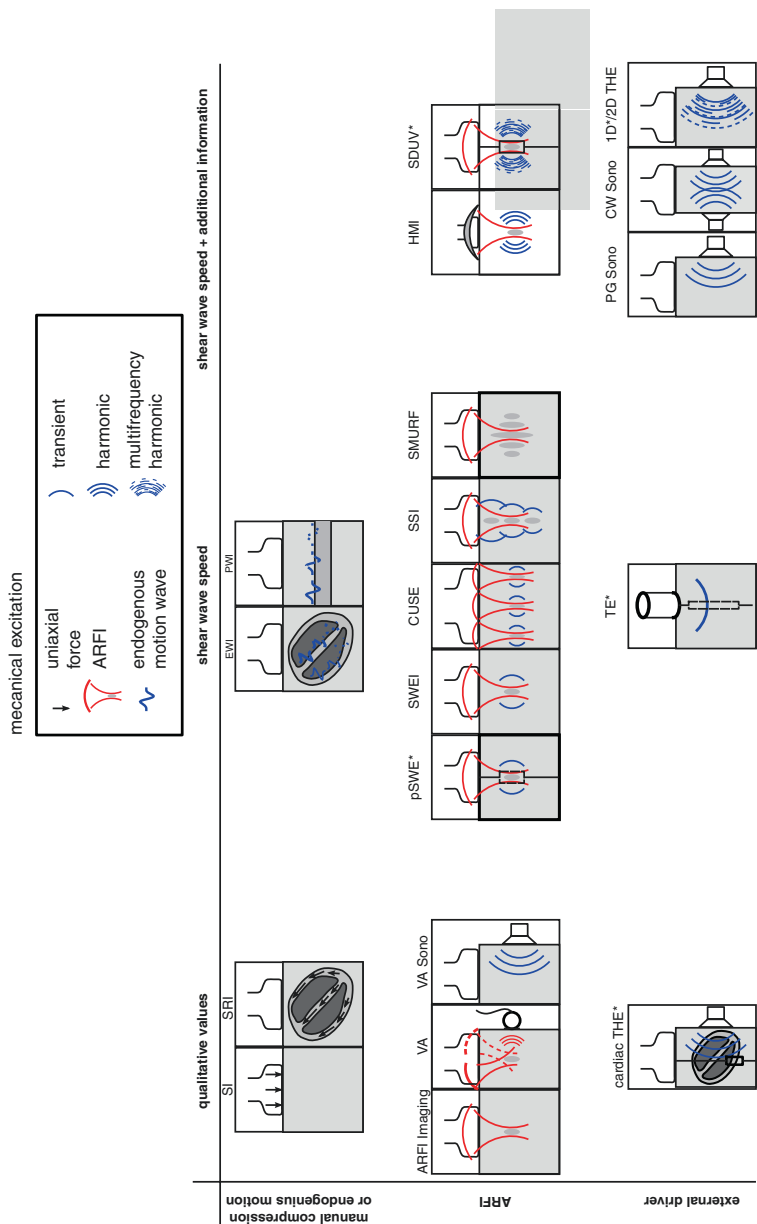


Fig. 12.4 Schematic overview of ultrasound elastography methods. Abbreviations of the names of USE methods correspond to section titles of Sect. 12.4, which explains the methods in greater detail. Compression waves are marked in red, whereas shear waves are marked in blue. Methods which provide a scalar parameter instead of an image are marked by “asterisk”. Note that loudspeakers generate both shear waves and compression waves; however, for brevity we here assume that in USE only the shear wave speed is measured

The *coherent plane-wave compounding* method compensates for this drawback in image quality of plane-wave imaging by combining several plane-wave images of different tilting angles [5–7]. The final image quality is comparable to that of conventional B-mode ultrasound while the frame rate is one order of magnitude higher (in the order of a few hundreds of hertz). As a limitation, the coherent plane-wave compounding technique makes high demands on scanner hardware.

12.4 Ultrasound Elastography Methods

Many USE methods are reviewed in the literature [2, 8–14]. In this chapter we will only briefly summarize most of the USE methods and their (potential) application in diagnostic imaging. Some of the methods described below are commercially available, while others are still in an experimental state. Most USE methods can be classified by the values they measure, either strain, shear wave speed, or dispersion. Dispersion denotes the frequency dependence of the shear wave speed. Additional parameters such as the nonlinearity or anisotropy are also addressed, but, due to the highly experimental nature of these methods, we do not discuss them. A schematic overview of USE methods is given in Fig. 12.4.

12.4.1 Strain Imaging (SI)

Strain imaging (SI) was developed by Ophir et al. and first presented in 1991 [15]. An overview is given in Varghese [16].

SI is based on quasi-static tissue deformations with a dynamical change far below 10 Hz. Quasi-static deformations can be induced by manually applying compression forces to the body surface or by exploiting internal excitation such as respiratory movements, cardiac motion, or vascular pulsation. The resulting axial or lateral tissue displacement, u , can be detected using the color mode. This displacement is the tissue movement between two consecutive frames or over the temporal integration of several frames. Tissue strain ε (see Chap. 2, Eq. (2.6)) can be calculated using the spatial derivative of the displacement. In one dimension

$$\varepsilon = \frac{\partial u}{\partial x}. \quad (12.2)$$

The resulting strain images are visualized as shown in Fig. 12.5. In general, the amount of force/stress applied to the tissue is unknown, and therefore SI is a qualitative elastography method, and only the relative shear modulus can be reconstructed [17]. Due to the simple and palpation-related setup, SI requires no special hardware but longer training periods.

SI is used for evaluation of the breasts, prostate, thyroid, muscle, and lymph nodes, and in principle, all organs accessible to manual palpation can be examined [16].

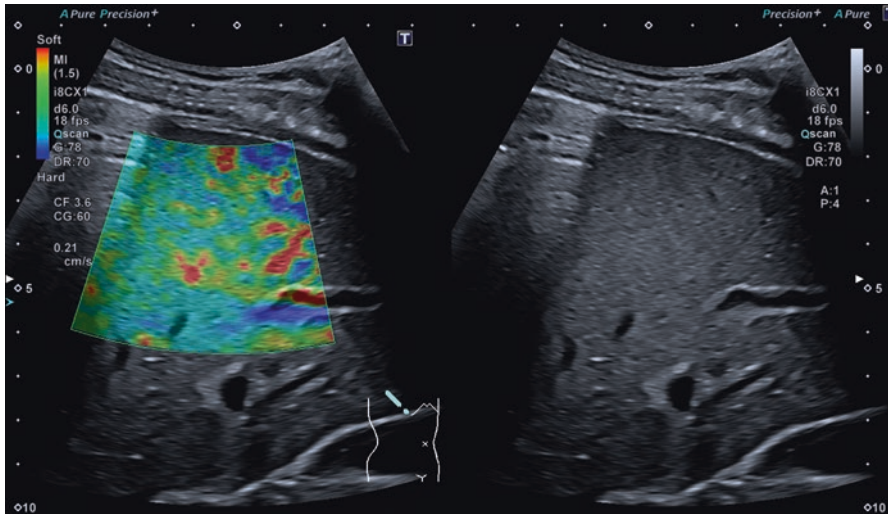


Fig. 12.5 Standard display of a liver examination by strain imaging using a Toshiba Aplio i900 ultrasound scanner (Toshiba, Otawara, Japan)

12.4.2 Strain Rate Imaging (SRI)

Strain rate imaging (SRI) is related to the cardiac Doppler measurement and therefore mainly used in echocardiography [18]. In contrast to SI, the basic measurement value is the tissue velocity $v = \dot{u}$, and therefore the strain rate $\dot{\epsilon}$ is displayed:

$$\dot{\epsilon} = \frac{\partial \dot{u}}{\partial x}. \quad (12.3)$$

Besides real-time tracking of the strain rate, the color mode-based values enable derivation of information on tissue dilatation ($\dot{\epsilon} > 0$) or contraction ($\dot{\epsilon} < 0$). SRI has been applied to intrinsic tissue deformation like in the heart, the muscle, or the gastrointestinal wall [8].

12.4.3 Acoustic Radiation Force Impulse (ARFI) Imaging

Acoustic radiation force impulse (ARFI) imaging is based on the work of Sarvazyan et al. [19] and was first published by Nightingale et al. [20] in 2002. An overview can be found in [21].

To avoid external tissue compression and to stimulate the tissue directly in the target region, ARFI uses highly focused ultrasound pulses to generate force/stress as explained above. The resulting deformation is in the order of tens of micrometers. Rapid acquisition of signals near the focus of the ARFI pulses provides information on strain, and the resulting images are comparable to SI. Due to the decreasing focus quality with increasing depth, ARFI is limited to approximately 8 cm depth.

ARFI imaging has been used to investigate abdominal organs, the breast, heart, vessels, nerve, and prostate and to monitor thermal ablation procedures [21].

12.4.4 Vibro-Acoustography (VA)

Vibro-acoustography (VA) was introduced by Fatemi and Greenleaf [22, 23] in 1998. An overview can be found in Urban et al. [24].

VA uses time-harmonic tissue excitation generated by two ARFI beams with slightly different ultrasonic frequencies. Within the focus region, a point source is generated with a difference frequency of typically 10–70 kHz. The amplitude of the emanating compression wave is detected by a hydrophone. The size of the compression wave amplitude is related to the tissue's stiffness. Spatial resolution in the field of view ($5 \times 5 \text{ cm}^2$) is achieved by sweeping the joint focus. Unlike ultrasound images, VA images are speckle free and highly sensitive to calcifications. It takes several minutes to scan a $5 \times 5 \text{ cm}^2$ image; however, this time can be reduced to 1 min using a linear transducer.

VA has been applied to the breast, thyroid, liver, ex vivo prostate, and porcine arteries [24].

12.4.5 Vibration Amplitude Sonoelastography (VA Sono)

Vibration amplitude sonoelastography (VA Sono) was developed by Lerner et al. [25] in 1988. An overview can be found in Parker [26].

VA Sono was the first ultrasound elastography method based on time-harmonic vibration. For this an external driver generates mono- or multifrequency excitation in the range of 20–1000 Hz. The resulting tissue displacement is captured by Doppler techniques, and the corresponding vibration amplitude is calculated using Fourier-Bessel functions. Like in ARFI imaging and VA, this amplitude provides qualitative information on tissue stiffness.

VA Sono has been used in the liver, breast, kidney, prostate, and eye and to characterize lesions [26].

12.4.6 Cardiac Time-Harmonic Elastography (Cardiac THE)

Cardiac time-harmonic elastography (cardiac THE) was developed by Tzschätzsch et al. [27] and presented in 2012.

Cardiac THE is based on observations made by cardiac magnetic resonance elastography showing that externally induced shear wave amplitudes in the left ventricle vary in synchrony with alterations in myocardial stiffness [28, 29]. The technical principles are similar to vibration amplitude sonoelastography (see Sect. 12.4.5). An external loudspeaker generates a 30 Hz vibration, and the resulting myocardial wall vibration is captured in the A-mode. The vibration amplitude, which is displayed in real time, shows mechanical tissue contraction during systole and tissue

relaxation during diastole by high and low values, respectively. Mechanical contraction and relaxation occur prior to the geometrical phases of the heart. The time delay between the wave amplitude alteration and heart geometry is a direct measure of isovolumetric times of the cardiac cycle [30]. Cardiac THE is currently under investigation for detecting cardiac diastolic dysfunction.

12.4.7 Electromechanical Wave Imaging (EWI)

Electromechanical wave imaging (EWI) was first published by Pernot and Konofagou [31] in 2005 and revised by Konofagou et al. [32].

EWI exploits the intrinsic electromagnetic activation of the heart muscle, which involves the generation of shear waves that propagate through the myocardium. These waves can be captured in the B-mode at a high frame rate of 500 frames/s. This is achieved by subdividing the color mode image into several sectors, which are consecutively acquired through the cardiac cycle. The isochrones are reconstructed in 3D based on the segmented strain image. Isochrones are hypothetical lines connecting sites where the activation signal at the tissue deflection due to electromechanical waves passes at the same time. In this way EWI visualizes the spreading of electromechanical activation across the myocardium. The feasibility of EWI has been demonstrated in canine tissue and humans [32]. An alternative approach based on the acoustic waves produced by heart sounds was developed by Kanai and Koiwa [33] in 2001. This method captures the shear wave generated by an aortic valve closure within the left ventricular septum. A high frame rate of 450 Hz is achieved by reducing the number of lines of sight to 16, and wave propagation is displayed in a time-distance plot whose slope indicates the shear wave speed [34].

12.4.8 Pulse Wave Imaging (PWI)

Pulse wave imaging (PWI) was published by Pernot et al. [35] in 2007, and an overview can be found in Konofagou et al. [32].

The pulse wave caused by cardiac contraction travels along the aorta as a bulk wave. The pulse wave velocity, c , is related to Young's modulus of the aortic wall, E , via the Moens-Korteweg equation [32]:

$$E = \frac{2 \rho R c^2}{b} \quad (12.4)$$

where ρ is the density of the aortic wall, R is the inner radius, and b is the thickness of the wall.

PWI is based on the findings of Kanai in 1994 [36] using Doppler ultrasound to measure the pulse wave displacement of the aortic wall at two lateral positions. From the displacements, the time of flight and finally Young's modulus are calculated.

To provide spatial resolution, Pernot et al. [35] used plane-wave imaging with up to 8000 frames/s to capture the pulse wave at multiple time points. Pulse wave velocity can be measured by a time-of-flight algorithm.

PWI has been applied to the aorta of mice and humans [32].

12.4.9 Point Shear Wave Elastography (pSWE)

Point shear wave elastography (pSWE) was developed by Palmeri et al. [37] in 2008. An overview is given in Bruno et al. [38].

The pSWE technique is also known as *ARFI quantification*. In contrast to ARFI quantification, tissue displacement is measured outside the excitation point (see Fig. 12.6). Furthermore, a time-of-flight algorithm estimates the mean speed from the spherically propagating shear wave, providing a quantitative value of intrinsic tissue properties.

pSWEI has been applied to the liver, spleen, kidney, pancreas, and thyroid [38].

12.4.10 Shear Wave Elasticity Imaging (SWEI)

Shear wave elasticity imaging (SWEI) was developed by Nightingale et al. [39] and presented in 2003. It is based on the principle of ARFI [19].

Tissue excitation in SWEI is similar to that in pSWEI except that a map of the shear wave speed (in the order of $3 \times 4 \text{ cm}^2$) is obtained by repeated ARFI excitations at different lateral positions. Similar to pSWEI, the wave speed is calculated using wave peak detection and a time-of-flight algorithm (see Fig. 12.7).

SWEI has been used for investigation of the liver, spleen, breast, and lymph nodes [40–42].

12.4.11 Comb-Push Ultrasound Shear Elastography (CUSE)

Comb-push ultrasound shear elastography (CUSE) was developed by Song et al. [43] and presented in 2012.

CUSE uses simultaneous ARFI excitation to overcome the limited frame rate of SWEI, which is due to repeated scanning at different lateral positions. Using simultaneous excitations and plane-wave imaging, CUSE acquires multiple shear waves within a few milliseconds. The displacement is estimated by a 2D autocorrelation algorithm. Directional filtering combined with a time-of-flight algorithm is used to reconstruct the elastogram in smaller regions (approximately $4 \times 4 \text{ cm}^2$).

The feasibility of CUSE was demonstrated in phantoms, in vivo thyroid, and breast tissue [44, 45].

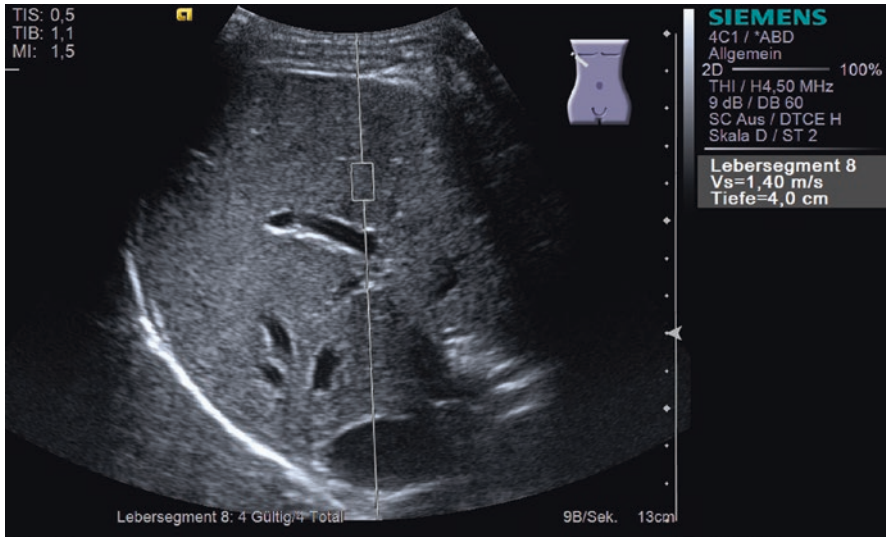


Fig. 12.6 Liver investigation by pSWEI using a Siemens Acuson S2000 ultrasound scanner (Siemens, Mountain View CA, USA). The ARFI focus and the corresponding shear wave speed of 1.40 m/s are obtained inside the rectangular region of interest

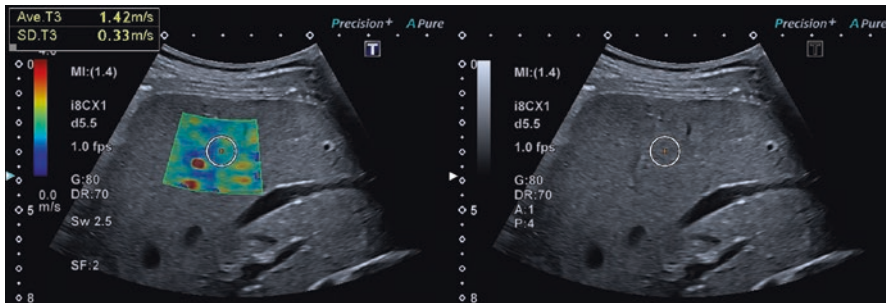


Fig. 12.7 Liver investigation by SWEI using a Toshiba Aplio i900 ultrasound scanner (Toshiba, Otawara, Japan). The mean shear wave speed within the selected ROI is 1.42 m/s

12.4.12 Supersonic Shear Imaging (SSI)

Supersonic shear imaging (SSI) was developed by Bercoff et al. [46] in 2004.

Spherically propagating shear waves from point sources as generated in pSWEI and SWEI can produce artifacts in the elastograms since most reconstruction methods assume plane-wave propagation. To generate plane waves, SSI applies repeated ARFI excitation at different focal depths. The foci are moved through the tissue with a higher speed than the shear wave speed, which gives rise to a Mach cone of nearly cylindrical geometry. The tissue displacement is captured with a frame rate of a few thousands of hertz by coherent plane-wave compounding. Shear wave

speed is calculated using a time-of-flight algorithm, and the final elastogram is displayed with a frame rate of 3–4 Hz.

SSI has been applied to many organs and tissues including the breast, liver, spleen, thyroid, prostate, skeletal muscle, and transplanted kidneys [13].

12.4.13 Spatially Modulated Ultrasound Radiation Force (SMURF)

Spatially modulated ultrasound radiation force (SMURF) was developed by McAleavey et al. [47] and presented in 2007.

Most elastography methods control the temporal behavior of tissue motion and analyze the spatial behavior of the motion to reconstruct elastic properties. In contrast, SMURF attempts to control the spatial behavior of motion by a laterally modulated ARFI pattern. This pattern determines the wavelength, λ , of the shear wave, while its oscillating frequency, f , is measured by $c = \lambda f$. SMURF uses a high pulse repetition rate for each image line since the transiently induced shear waves are rapidly attenuated due to geometrical and viscous dispersion. SMURF was demonstrated in phantoms and an ex vivo porcine liver tissue [47, 48].

12.4.14 Transient Elastography (TE)

Transient elastography (TE) was developed by Sandrin et al. [49] for noninvasively staging liver fibrosis and presented in 2002.

In TE the tissue is excited by an external piston driver operated with a burst of a single 50 Hz vibration cycle. The generated shear wave propagates from the skin surface into deeper tissue and is captured in the M-mode. The shear wave fronts appear in the time-depth plot of the M-mode as parallel lines whose slope is the shear wave speed (see Fig. 12.8). TE provides a mean value for shear wave speed without spatial resolution. Similar to ARFI-based methods, TE is limited to a maximum depth of approx. 8 cm. TE was one of the first commercially available ultrasound elastography methods and is therefore best validated. Due to the lack of B-mode guidance, positioning the M-mode beam can be challenging.

The main application of TE is the staging of liver fibrosis. However, TE has also been tested in the breast, skeletal muscles, skin, and blood clots [13].

12.4.15 Harmonic Motion Imaging (HMI)

Harmonic motion imaging (HMI) was developed by Konofagou and Hynynen [50] and presented in 2003. An overview is given in Konofagou et al. [51].

The motivation for the development of HMI was the observation of changes in viscoelastic properties during thermal ablation with *high-intensity focused ultrasound* (HIFU). In contrast to other elastography techniques, HMI allows evaluation of tissue behavior during HIFU ablation in real time which is useful to control the

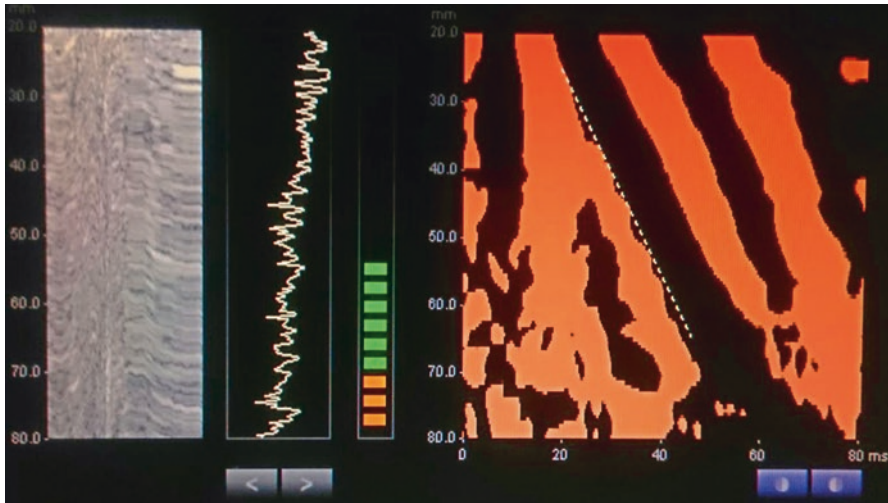


Fig. 12.8 Liver investigation by TE using a FibroScan® ultrasound scanner (Echosens, Paris, France). From left to right, M-mode, A-mode, feedback-color bar for contact pressure, and time-depth images of the shear wave with fitted slope (dashed white line)

duration of the ablation procedure. HMI is accomplished by amplitude modulation of the HIFU beam, which generates a harmonic vibration in the order of 50 Hz. Tissue deflection is captured using a second image transducer, embedded in the HIFU transducer. The necessary frame rate of a few hundreds of hertz is achieved by reducing the number of lines of sight. After temporal Fourier transformation, a phase gradient algorithm calculates the shear wave speed in the focus. As additional information, the phase shift between the vibration excitation and the measured tissue vibration is captured. This phase shift is identical to the phase angle of the complex-valued shear modulus. HMI is used for detection of breast cancer and other lesions and for real-time monitoring of thermal ablation [51].

12.4.16 Shear Wave Dispersion Ultrasound Vibrometry (SDUV)

Shear wave dispersion ultrasound vibrometry (SDUV) was developed by Chen et al. [52] and presented in 2004. An overview is given by Urban et al. [53].

Most ultrasound elastography methods measure only the shear wave phase velocity at one frequency or the group velocity of a transient burst. Additional information on viscosity can be obtained by evaluating the frequency dependence of shear wave speed (dispersion). Therefore SDUV excites harmonic vibration by ARFI at a base frequency and also at higher harmonics, which are typically in the range of 200–800 Hz. The superimposed tissue deflection is captured and frequency decomposed using Kalman filtering. For each frequency, the shear wave phase is evaluated at two lateral positions. The corresponding shear wave speed is calculated from this phase shift. Viscoelastic tissue properties can be reconstructed by fitting the Kelvin-Voigt model to the shear wave speed dispersion curve.

SDUV was used to investigate the skeletal muscle, liver, excised arteries, excised prostates, and excised porcine kidney [53].

A variant of SDUV, termed *Lamb wave dispersion ultrasound vibrometry* (LDUV), was used to investigate porcine myocardium during an open chest surgery [54].

12.4.17 Vibration Phase Gradient (PG) Sonoelastography

Vibration phase gradient (PG) sonoelastography is based on vibration amplitude sonoelastography and was developed by Yamakoshi et al. [55] and presented in 1990. An overview is given by Parker [26].

Tissue excitation and acquisition of the deflection are similar to vibration amplitude sonoelastography (see Sect. 12.4.5). In addition to the vibration amplitude, the vibration phase is captured, which allows quantification of shear wave speed using a phase gradient algorithm. When the tissue is stimulated by multifrequency excitation, PG sonoelastography can measure the dispersion of the shear wave speed.

PG sonoelastography was demonstrated in the skeletal muscle [26].

12.4.18 Crawling Waves (CW) Sonoelastography

Crawling waves (CW) sonoelastography was developed by Wu et al. [56] and presented in 2004. A review is given by Parker [26].

CW sonoelastography was developed to overcome limitations with regard to the frame rate of normal clinical scanners used for PG sonoelastography. Since the oscillation frequency f of time-harmonic shear waves in elastography is in the order of the frame rate of commercial ultrasound devices (approx. 80 Hz), the propagation of shear waves cannot be captured directly without aliasing artifacts. Therefore, CW sonoelastography uses two loudspeakers which are placed at opposite sides of the tissue and which have a slightly different vibration frequency, $f + \Delta f$ and $f - \Delta f$, with $\Delta f \ll f$. The resulting interference pattern is composed of a wave with two apparent wavelengths ($\lambda_1 = \Delta f/c$ and $\lambda_2 = f/c$) oscillating at two vibration frequencies (f and Δf). The apparent wave with wavelength λ_1 and oscillation frequency Δf meets the criteria to be captured by low frame rates while being suitable for inversion techniques since wavelengths are short ($\lambda_1 \ll \lambda_2$). Using multifrequency excitation CW sonoelastography is able to measure shear wave dispersion. CW sonoelastography with external loudspeakers was applied to ex vivo prostate and liver tissue [26] and demonstrated in vivo in the skeletal muscle [57–59].

12.4.19 Time-Harmonic Elastography (1D/2D THE)

Time-harmonic elastography (THE) is similar to vibration phase gradient sonoelastography except that it uses multiple harmonic drive frequencies and compound shear wave speed mapping [60].

THE uses a loudspeaker integrated into a patient bed and operated by a superposition of harmonic signals in the frequency range between 30 and 60 Hz. In 1D THE, the resulting tissue displacement is captured in the M-mode along multiple profiles corresponding to varying transducer positions. A fit-based algorithm automatically selects the most reliable wave speed values and evaluates the dispersion of shear wave speed.

2D THE also uses multifrequency wave stimulations. However, since motion is captured by a standard B-mode scanner with frame rates in the order of 80 Hz, vibrations slightly above the Nyquist limit are evaluated at aliasing frequency. Compound maps of wave speed are reconstructed by multifrequency inversion of directionally filtered wave images [61]. 2D THE is less limited in penetration depth than other methods and provides an elastogram which covers the entire B-mode image. A similar compounding reconstruction technique, *external vibration multidirectional ultrasound shear wave elastography* (EVMUSE), was proposed by Zhao et al. [62]. However, in EVMUSE, a single-frequency 50 Hz wave is observed a few milliseconds after vibration is stopped, giving rise to some transient wave effects.

1D THE was used in healthy volunteers [60, 63, 64], in liver fibrosis staging [65], and for evaluating liver decompression after shunt implantation [66]. Feasibility of 2D THE was demonstrated for liver and spleen examinations in volunteers [61].

Conclusion

Despite widespread clinical applications of USE, consistent thresholds and standardized stiffness-based diagnostic indices are still lacking. The discrepant results of USE studies are mainly attributable to the fact that so many different techniques are used. This is exactly the boon and bane of a rapidly developing and highly innovative field such as USE. On the one hand, new USE methods offer more insight into tissue mechanical parameters in health and disease. On the other hand, research groups and manufactures worldwide are inclined to validate their own methods for self-consistency instead of searching for modality-independent quantitative and tissue-inherent parameters. The importance of modality-independent and quantitative imaging biomarkers has been recognized and addressed by many alliances worldwide including the *Quantitative Imaging Biomarkers Alliance* (QIBA) or the *European Imaging Biomarkers Alliance* (EIBALL). The rapid progress made by USE promises that one day a gold standard of mechanical tissue properties will be developed, to which new methods can be compared. One promising approach is time-harmonic elastography (THE), which measures stiffness at well-defined excitation frequencies and which can thus be compared with reference methods such as MRI elastography. There is no doubt that well-documented standards in elastography will foster the dissemination of mechanical imaging biomarkers and thus contribute to higher precision of ultrasound-based diagnoses.

References

1. Tzschätzsch H. Entwicklung, anwendung und validierung der zeitharmonischen in vivo ultraschallelastografie an der menschlichen leber und am menschlichen herzen. Dissertation. Humboldt Universität Berlin. 2016.
2. Sarvazyan AP, Urban MW, Greenleaf JF. Acoustic waves in medical imaging and diagnostics. *Ultrasound Med Biol.* 2013;39(7):1133–46. <https://doi.org/10.1016/j.ultrasmedbio.2013.02.006>.
3. Sugimoto T, Ueha S, Itoh K. Tissue hardness measurement using the radiation force of focused ultrasound. In: *IEEE symposium on ultrasonics.* IEEE; 1990. p. 1377–1380. <https://doi.org/10.1109/ULTSYM.1990.171591>.
4. Lu JY. 2D and 3D high frame rate imaging with limited diffraction beams. *IEEE Trans Ultrason Ferroelectr Freq Control.* 1997;44(4):839–56. <https://doi.org/10.1109/58.655200>.
5. Cheng J, Lu J. Extended high-frame rate imaging method with limited-diffraction beams. *IEEE Trans Ultrason Ferroelectr Freq Control.* 2006;53(5):880–99. <https://doi.org/10.1109/TUFFC.2006.1632680>.
6. Montaldo G, Tanter M, Bercoff J, Benech N, Fink M. Coherent plane-wave compounding for very high frame rate ultrasonography and transient elastography. *IEEE Trans Ultrason Ferroelectr Freq Control.* 2009;56(3):489–506. <https://doi.org/10.1109/TUFFC.2009.1067>.
7. Song TK, Chang JH. Synthetic aperture focusing method for ultrasound imaging based on planar waves. 2004.
8. Bamber J, Cosgrove D, Dietrich C, Fromageau J, Bojunga J, Calliada F, et al. EFSUMB guidelines and recommendations on the clinical use of ultrasound elastography. Part 1: basic principles and technology. *Ultraschall Med.* 2013;34(2):169–84. <https://doi.org/10.1055/s-0033-1335205>.
9. Cosgrove D, Piscaglia F, Bamber J, Bojunga J, Correas J-M, Gilja O, et al. EFSUMB guidelines and recommendations on the clinical use of ultrasound elastography. Part 2: clinical applications. *Ultraschall Med.* 2013;34(3):238–53. <https://doi.org/10.1055/s-0033-1335375>.
10. Greenleaf JF, Fatemi M, Insana M. Selected methods for imaging elastic properties of biological tissues. *Annu Rev Biomed Eng.* 2003;5(1):57–78. <https://doi.org/10.1146/annurev.bioeng.5.040202.121623>.
11. Parker KJ, Doyley MM, Rubens DJ. Corrigendum: imaging the elastic properties of tissue: the 20 year perspective. *Phys Med Biol.* 2012;57(16):5359–60. <https://doi.org/10.1088/0031-9155/57/16/5359>.
12. Parker KJ, Taylor LS, Gracewski S, Rubens DJ. A unified view of imaging the elastic properties of tissue. *J Acoust Soc Am.* 2005;117(5):2705. <https://doi.org/10.1121/1.1880772>.
13. Sarvazyan A, Hall TJ, Urban MW, Fatemi M, Aglyamov SR, Garra BS. An overview of Elastography - an emerging branch of medical imaging. *Curr Med Imaging Rev.* 2011;7(4):255–82. <https://doi.org/10.2174/157340511798038684>.
14. Zaleska-Dorobisz U, Kaczorowski K, Pawluś A, Puchalska A, Inglot M. Ultrasound elastography - review of techniques and its clinical applications. *Adv Clin Exp Med.* 2014;23(4):645–55. Retrieved from <http://www.ncbi.nlm.nih.gov/pubmed/25166452>
15. Ophir J. Elastography: a quantitative method for imaging the elasticity of biological tissues. *Ultrason Imaging.* 1991;13(2):111–34. [https://doi.org/10.1016/0161-7346\(91\)90079-W](https://doi.org/10.1016/0161-7346(91)90079-W).
16. Varghese T. Quasi-static ultrasound elastography. *Ultrasound Clin.* 2009;4(3):323–38. <https://doi.org/10.1016/j.cult.2009.10.009>.
17. Oberai AA, Gokhale NH, Goenezen S, Barbone PE, Hall TJ, Sommer AM, Jiang J. Linear and nonlinear elasticity imaging of soft tissue in vivo: demonstration of feasibility. *Phys Med Biol.* 2009;54(5):1191.
18. Fleming AD, Xia X, McDicken WN, Sutherland GR, Fenn L. Myocardial velocity gradients detected by Doppler imaging. *Br J Radiol.* 1994;67(799):679–88. <https://doi.org/10.1259/0007-1285-67-799-679>.

19. Sarvazyan AP, Rudenko OV, Swanson SD, Fowlkes JB, Emelianov SY. Shear wave elasticity imaging: a new ultrasonic technology of medical diagnostics. *Ultrasound Med Biol.* 1998;24(9):1419–35. [https://doi.org/10.1016/S0301-5629\(98\)00110-0](https://doi.org/10.1016/S0301-5629(98)00110-0).
20. Nightingale K, Soo MS, Nightingale R, Trahey G. Acoustic radiation force impulse imaging: in vivo demonstration of clinical feasibility. *Ultrasound Med Biol.* 2002;28(2):227–35. [https://doi.org/10.1016/S0301-5629\(01\)00499-9](https://doi.org/10.1016/S0301-5629(01)00499-9).
21. Nightingale K. Acoustic radiation force impulse (ARFI) imaging: a review. *Curr Med Imaging Rev.* 2012;7(4):328–39. <https://doi.org/10.2174/157340511798038657>.
22. Fatemi M. Ultrasound-stimulated vibro-acoustic spectrography. *Science.* 1998;280(5360):82–5. <https://doi.org/10.1126/science.280.5360.82>.
23. Fatemi M, Greenleaf JF. Vibro-acoustography: an imaging modality based on ultrasound-stimulated acoustic emission. *Proc Natl Acad Sci.* 1999;96(12):6603–8. <https://doi.org/10.1073/pnas.96.12.6603>.
24. Urban MW, Alizad A, Aquino W, Greenleaf JF, Fatemi M. A review of vibro-acoustography and its applications in medicine. *Curr Med Imaging Rev.* 2011;7(4):350–9. <https://doi.org/10.2174/157340511798038648>.
25. Lerner RM, Parker KJ, Hohen J, Gramiak R, Waag RC. Sono-elasticity: medical elasticity images derived from ultrasound signals in mechanically vibrated targets. *Acoust Imaging.* 1988;16:317–27. https://doi.org/10.1007/978-1-4613-0725-9_31.
26. Parker KJ. The evolution of vibration sonoelastography. *Curr Med Imaging Rev.* 2011;7(4):283–91. <https://doi.org/10.2174/157340511798038675>.
27. Tzschätzsch H, Elgeti T, Rettig K, Kargel C, Klaua R, Schultz M, et al. In vivo time harmonic elastography of the human heart. *Ultrasound Med Biol.* 2012;38(2):214–22. <https://doi.org/10.1016/j.ultrasmedbio.2011.11.002>.
28. Elgeti T, Beling M, Hamm B, Braun J, Sack I. Elasticity-based determination of isovolumetric phases in the human heart. *J Cardiovasc Magn Reson.* 2010;12(1):60. <https://doi.org/10.1186/1532-429X-12-60>.
29. Sack I, Rump J, Elgeti T, Samani A, Braun J. MR elastography of the human heart: noninvasive assessment of myocardial elasticity changes by shear wave amplitude variations. *Magn Reson Med.* 2009;61(3):668–77. <https://doi.org/10.1002/mrm.21878>.
30. Tzschätzsch H, Hättasch R, Knebel F, Klaua R, Schultz M, Jenderka K-V, et al. Isovolumetric elasticity alteration in the human heart detected by in vivo time-harmonic elastography. *Ultrasound Med Biol.* 2013;39(12):2272–8. <https://doi.org/10.1016/j.ultrasmedbio.2013.07.003>.
31. Pernot M, Konofagou EE. Electromechanical imaging of the myocardium at normal and pathological states. *IEEE Ultrason Symp.* 2005;2:1091–4. <https://doi.org/10.1109/ULTSYM.2005.1603040>.
32. Konofagou E, Lee W-N, Luo J, Provost J, Vappou J. Physiologic cardiovascular strain and intrinsic wave imaging. *Annu Rev Biomed Eng.* 2011;13(1):477–505. <https://doi.org/10.1146/annurev-bioeng-071910-124721>.
33. Kanai H, Koiwa Y. Myocardial rapid velocity distribution. *Ultrasound Med Biol.* 2001;27(4):481–98. [https://doi.org/10.1016/S0301-5629\(01\)00341-6](https://doi.org/10.1016/S0301-5629(01)00341-6).
34. Kanai H. Propagation of vibration caused by electrical excitation in the normal human heart. *Ultrasound Med Biol.* 2009;35(6):936–48. <https://doi.org/10.1016/j.ultrasmedbio.2008.12.013>.
35. Pernot M, Fujikura K, Fung-Kee-Fung SD, Konofagou EE. ECG-gated, mechanical and electromechanical wave imaging of cardiovascular tissues in vivo. *Ultrasound Med Biol.* 2007;33(7):1075–85. <https://doi.org/10.1016/j.ultrasmedbio.2007.02.003>.
36. Kanai H, Kawabe K, Takano M, Murata R, Chubachi N, Koiwa Y. New method for evaluating local pulse wave velocity by measuring vibrations on arterial wall. *Electron Lett.* 1994;30(7):534–6. <https://doi.org/10.1049/el:19940393>.
37. Palmeri ML, Wang MH, Dahl JJ, Frinkley KD, Nightingale KR. Quantifying hepatic shear modulus in vivo using acoustic radiation force. *Ultrasound Med Biol.* 2008;34(4):546–58. <https://doi.org/10.1016/j.ultrasmedbio.2007.10.009>.
38. Bruno C, Minniti S, Mucell BA, Roberto P. ARFI: from basic principles to clinical applications in diffuse chronic disease—a review. *Insights Imaging.* 2016;7:735–46.

39. Nightingale K, McAleavey S, Trahey G. Shear-wave generation using acoustic radiation force: in vivo and ex vivo results. *Ultrasound Med Biol.* 2003;29(12):1715–23. <https://doi.org/10.1016/j.ultrasmedbio.2003.08.008>.
40. Cheng KL, Choi YJ, Shim WH, Lee JH, Baek JH. Virtual touch tissue imaging quantification shear wave elastography: prospective assessment of cervical lymph nodes. *Ultrasound Med Biol.* 2016;42(2):378–86. <https://doi.org/10.1016/j.ultrasmedbio.2015.10.003>.
41. Ianculescu V, Ciolovan LM, Dunant A, Vielh P, Mazouni C, Delaloue S, et al. Added value of virtual touch IQ shear wave elastography in the ultrasound assessment of breast lesions. *Eur J Radiol.* 2014;83(5):773–7.
42. Leschied JR, Dillman JR, Bilhartz J, Heider A, Smith EA, Lopez MJ. Shear wave elastography helps differentiate biliary atresia from other neonatal/infantile liver diseases. *Pediatr Radiol.* 2015;45(3):366–75. <https://doi.org/10.1007/s00247-014-3149-z>.
43. Song P, Zhao H, Manduca A, Urban MW, Greenleaf JF, Chen S. Comb-push ultrasound shear elastography (CUSE): a novel method for two-dimensional shear elasticity imaging of soft tissues. *IEEE Trans Med Imaging.* 2012;31(9):1821–32. <https://doi.org/10.1109/TMI.2012.2205586>.
44. Mehrmohammadi M, Song P, Meixner DD, Fazzio RT, Chen S, Greenleaf JF, et al. Comb-push ultrasound shear elastography (CUSE) for evaluation of thyroid nodules: preliminary in vivo results. *IEEE Trans Med Imaging.* 2015;34(1):97–106. <https://doi.org/10.1109/TMI.2014.2346498>.
45. Denis M, Mehrmohammadi M, Song P, Meixner DD, Fazzio RT, Pruthi S, et al. Comb-push ultrasound shear elastography of breast masses: initial results show promise. *PLoS One.* 2015;10(3):e0119398. <https://doi.org/10.1371/journal.pone.0119398>.
46. Bercoff J, Tanter M, Fink M. Supersonic shear imaging: a new technique for soft tissue elasticity mapping. *IEEE Trans Ultrason Ferroelectr Freq Control.* 2004;51(4):396–409. <https://doi.org/10.1109/TUFFC.2004.1295425>.
47. McAleavey SA, Menon M, Orszulak J. Shear-modulus estimation by application of spatially-modulated impulsive acoustic radiation force. *Ultrason Imaging.* 2007;104(2007):87–104.
48. McAleavey S, Menon M, Elegbe E. Shear modulus imaging with spatially-modulated ultrasound radiation force. *Ultrason Imaging.* 2009;31(4):217–34. <https://doi.org/10.1177/016173460903100403>.
49. Sandrin L, Tanter M, Gennisson J-L, Catheline S, Fink M. Shear elasticity probe for soft tissues with 1-D transient elastography. *IEEE Trans Ultrason Ferroelectr Freq Control.* 2002;49(4):436–46. <https://doi.org/10.1109/58.996561>.
50. Konofagou EE, Hynynen K. Localized harmonic motion imaging: theory, simulations and experiments. *Ultrasound Med Biol.* 2003;29(10):1405–13. [https://doi.org/10.1016/S0301-5629\(03\)00953-0](https://doi.org/10.1016/S0301-5629(03)00953-0).
51. Konofagou EE, Maleke C, Vappou J. Harmonic motion imaging (HMI) for tumor imaging and treatment monitoring. *Curr Med Imaging Rev.* 2012;8:16. <https://doi.org/10.2174/157340512799220616>.
52. Chen S, Fatemi M, Greenleaf JF. Quantifying elasticity and viscosity from measurement of shear wave speed dispersion. *J Acoust Soc Am.* 2004;115(6):2781. <https://doi.org/10.1121/1.1739480>.
53. Urban MW, Chen S, Fatemi M. A review of shearwave dispersion ultrasound vibrometry (SDUV) and its applications. *Curr Med Imaging Rev.* 2012;8(1):27–36. <https://doi.org/10.2174/157340512799220625>.
54. Nenadic IZ, Urban MW, Mitchell SA, Greenleaf JF. Lamb wave dispersion ultrasound vibrometry (LDUV) method for quantifying mechanical properties of viscoelastic solids. *Phys Med Biol.* 2011;56(7):2245–64. <https://doi.org/10.1088/0031-9155/56/7/021>.
55. Yamakoshi Y, Sato J, Sato T. Ultrasonic imaging of internal vibration of soft tissue under forced vibration. *IEEE Trans Ultrason Ferroelectr Freq Control.* 1990;37(2):45–53. <https://doi.org/10.1109/58.46969>.
56. Wu Z, Taylor LS, Rubens DJ, Parker KJ. Sonoelastographic imaging of interference patterns for estimation of the shear velocity of homogeneous biomaterials. *Phys Med Biol.* 2004;49(6):911–22. <https://doi.org/10.1088/0031-9155/49/6/003>.

57. Hazard C, Hah Z, Rubens D, Parker K. Integration of crawling waves in an ultrasound imaging system. Part 1: system and design considerations. *Ultrasound Med Biol.* 2012;38(2):296–311. <https://doi.org/10.1016/j.ultrasmedbio.2011.10.026>.
58. Hah Z, Hazard C, Mills B, Barry C, Rubens D, Parker K. Integration of crawling waves in an ultrasound imaging system. Part 2: signal processing and applications. *Ultrasound Med Biol.* 2012;38(2):312–23. <https://doi.org/10.1016/j.ultrasmedbio.2011.10.014>.
59. Hoyt K, Castaneda B, Parker KJ. Two-dimensional sonoelastographic shear velocity imaging. *Ultrasound Med Biol.* 2008;34(2):276–88. <https://doi.org/10.1016/j.ultrasmedbio.2007.07.011>.
60. Tzschätzsch H, Ipek-Ugay S, Guo J, Streitberger K-J, Gentz E, Fischer T, et al. In vivo time-harmonic multifrequency elastography of the human liver. *Phys Med Biol.* 2014;59(7):1641–54. <https://doi.org/10.1088/0031-9155/59/7/1641>.
61. Tzschätzsch H, Nguyen Trong M, Scheuermann T, Fischer T, Schultz M, Braun J, Sack I. Two-dimensional time-harmonic elastography of the human liver and spleen. *Ultrasound Med Biol.* 2016;16:30163–6. <https://doi.org/10.1016/j.ultrasmedbio.2016.07.004>.
62. Zhao H, Song P, Meixner DD, Kinnick RR, Callstrom MR, Sanchez W, et al. External vibration multi-directional ultrasound shearwave elastography (EVMUSE): application in liver fibrosis staging. *IEEE Trans Med Imaging.* 2014;33(11):2140–8. <https://doi.org/10.1109/TMI.2014.2332542>.
63. Ipek-Ugay S, Tzschätzsch H, Braun J, Fischer T, Sack I. Physiological reduction of hepatic venous blood flow by Valsalva maneuver decreases liver stiffness. *J Ultrasound Med.* 2017;36:1305.
64. Ipek-Ugay S, Tzschätzsch H, Hudert C, Marticorena Garcia SR, Fischer T, Braun J, et al. Time harmonic elastography reveals sensitivity of liver stiffness to water ingestion. *Ultrasound Med Biol.* 2016;42(6):1289–94. <https://doi.org/10.1016/j.ultrasmedbio.2015.12.026>.
65. Tzschätzsch H, Ipek-Ugay S, Nguyen Trong M, Guo J, Eggers J, Gentz E, et al. Multifrequency time-harmonic elastography for the measurement of liver viscoelasticity in large tissue windows. *Ultrasound Med Biol.* 2015;41(3):724–33. <https://doi.org/10.1016/j.ultrasmedbio.2014.11.009>.
66. Tzschätzsch H, Sack I, Marticorena Garcia SR, Ipek-Ugay S, Braun J, Hamm B, Althoff CE. Time-harmonic elastography of the liver is sensitive to intrahepatic pressure gradient and liver decompression following transjugular intrahepatic portosystemic shunt (TIPS) implantation. *Ultrasound Med Biol.* 2017;43:595.